Modeling indoor aerosols transport

Xinyu Si

Abstract

Aerosols are among the most important carriers of hazardous chemicals and microorganisms indoor. Due to the small size, they can transport with wind to a significantly long distance. The size of aerosol particles and environmental factors can both considerably influence their transport behaviors. However, both particle sizes and environmental conditions can be considerably variable, which causes the complexity of this problem. The diameter of aerosol droplets can vary from millimeter to micron scale. The temperature can be uniform, increasing or decreasing with height. Therefore, it is meaningful to understand the transport properties of aerosols with different sizes in different environment conditions. In this report, a 2-D zero-equation aerosol transport model was built with constant logarithmic wind profile and parabolic eddy-viscosity. The behaviors of aerosols with different Rouse numbers (Ro) were tested. Meanwhile, the effect of temperature stratification was explored.

The result shows that the concentration of aerosols at fixed height will first increase and then decrease. Larger aerosol droplets will reach the peak concentration earlier. Smaller droplets can be much more persistent in the air than larger ones. A temperature inversion layer can effectively prevent the aerosols from crossing and moving upward.

1. Introduction

Aerosols are ubiquitous in industrial and environmental processes, indoors and outdoors [1]. They can be important carriers of various chemical compounds and microorganisms, hence contribute significantly to the transport of airborne and waterborne diseases. Understanding indoor aerosol transport is of great significance in modern society to improve the safety as well as comfort of living and working environment. For example, in hospital, it is crucial to prevent the aerosols generated from instrument cleaning that may contain fatal pathogens from leaking out of the safe zone.

Indoor aerosols are most commonly generated by various kinds of fragmentation processes, among which one of the most common categories is the bursting of bubbles at water-air interface.

A single bursting surface bubble can generate thousands of droplets, the size of which can be as small as micron scale. Due to the small size of these droplets, they can persist in the air for a long time and be transported by mean wind advection, diffusion, and turbulence dispersion to almost everywhere in the room.

On the one hand, the sizes of the aerosol droplets can significantly determine their transport properties. The smaller the droplets are, the easier can they be carried by wind to a further distance. The experiment of Villermaux et al. [2] shows that the number N and mean droplets diameter d_p are estimated to be controlled by the bubble cap radius R and film thickness at the burst h_b as

$$N \sim \left(\frac{R}{l_c}\right)^2 \left(\frac{R}{h_b}\right)^{\frac{7}{8}}, \tag{1}$$

$$d_p \sim R^{\frac{3}{8}} h_b^{\frac{5}{8}}, \tag{2}$$

where $l_c = \sqrt{\sigma/\rho g}$ is the capillary length, with σ the water surface tension, ρ the water density, and g the gravitational acceleration. Depending on different bubble sizes and bursting film thicknesses, the diameter of the generated droplets can vary from millimeter scale to micron scale. The experiment of Poulain et al. [3] shows that bubbles polluted with bacterial secretions can produce smaller and more numerous droplets than those produced by clean tap-water-bubbles, which enhances the transport property of these small particles, and results in an even severer concern.

The particle size can be evaluated by the nondimensional particle diameter

$$\mathrm{d_*} = \mathrm{d_p}\left[\frac{(s-1)g}{\nu^2}\right]^{1/3},$$

where s = 816.3 is the specific gravity of water versus air, and $\nu = 1.5 \times 10^{-5}$ $(\mathrm{m^2/s})$ is the kinematic viscosity of air at $25°C$. When $\mathrm{d_*}$ << 10, it is reasonable to approximate the settling velocity $\mathrm{w_p}$ with the Stokes settling velocity $(s-1)gd_p^2/(18\nu)$.

The balance between the inertia of a particle from gravitational force and the raising force from wind shear can be evaluated by a dimensionless group named Rouse number which is defined by

$$\mathrm{Ro} = \frac{\mathrm{w_p}}{\kappa \mathrm{u_*}},$$

where κ = 0.41 is the von Karman constant, and u_* is the friction velocity. Smaller Ro means the particle motion is shear dominant, hence they are easier to be picked up rather than deposit to the lower bed.

On the other hand, environmental factors, for example, temperature stratification, can also impact aerosol transport. A temperature inversion can effectively suppress the generation of turbulence, hence prevent the materials at lower altitude from moving upward. The effect of stratification can be evaluated by a dimensionless group named gradient Richardson number which is defined by

$$Ri = \frac{g\alpha\frac{\partial T}{\partial z}}{\left(\frac{\partial u}{\partial z}\right)^2} = \frac{Buoyancy^2}{Shear^2},$$

with $\alpha = 2.8 \times 10^{-3} K^{-1}$ the thermal expansion coefficient of air, and T the temperature. Larger Ri value means a stronger buoyancy effect restricting the shear from producing turbulence. For indoor environment, it is reasonable to assume a zero vertical mean wind, so the major cause of vertical aerosol transport is turbulent dispersion. If the vertical temperature gradient is large enough, it is possible to produce a safer upper zone by producing a temperature inversion indoor to suppress turbulence.

In this report, the influences of particle size and temperature stratification were explored with a 2-D, zero-equation aerosol transport model. Section 2 introduces the setup of the model and the governing equations used to model mean wind profile, turbulent dispersion, and temperature stratification. Section 3.1 shows how the varied Ro can affect the concentration distribution after reaching steady state. Section 3.2 shows how the temperature stratification can affect the horizontal and vertical transport of aerosols with a continuous or pulse source. Finally, section 4 summarizes this project and discusses the improvements could be made in the future to gain more insight into these topics.

2. Model overview and setup

The 2-D, uniform grid, zero-equation aerosol transport model was built with a 10 m length (L), 3 m height (H), and unit width space, in which each grid size was 0.1 m × 0.1 m ($\Delta x \times \Delta z$). The time step (Δt) was chosen to be 0.5s to keep the model stable. As figure (1a) shows, a point source was established at the very left cell at the bottom (referred as the source cell hereafter). Meanwhile, 6 measurement points were deployed at the quarter points at height 1.0 m and 1.8 m

respectively, which approximate the heights of adults and small children. The initial condition of concentration C (in the form of number density) was zero everywhere except for the source cell, at which $\tilde{C} = N/(\Delta x \Delta z) = 2.2 \times 10^5\ m^{-3}$, where N was calculated by equation (1) assuming R = 5 mm and h = 3 μm. When the source is referred as 'continuous' in this report, it emits N droplets at the source cell every 0.5s (1 time step). When referred as 'pulse', it will not emit aerosols after the first time step.

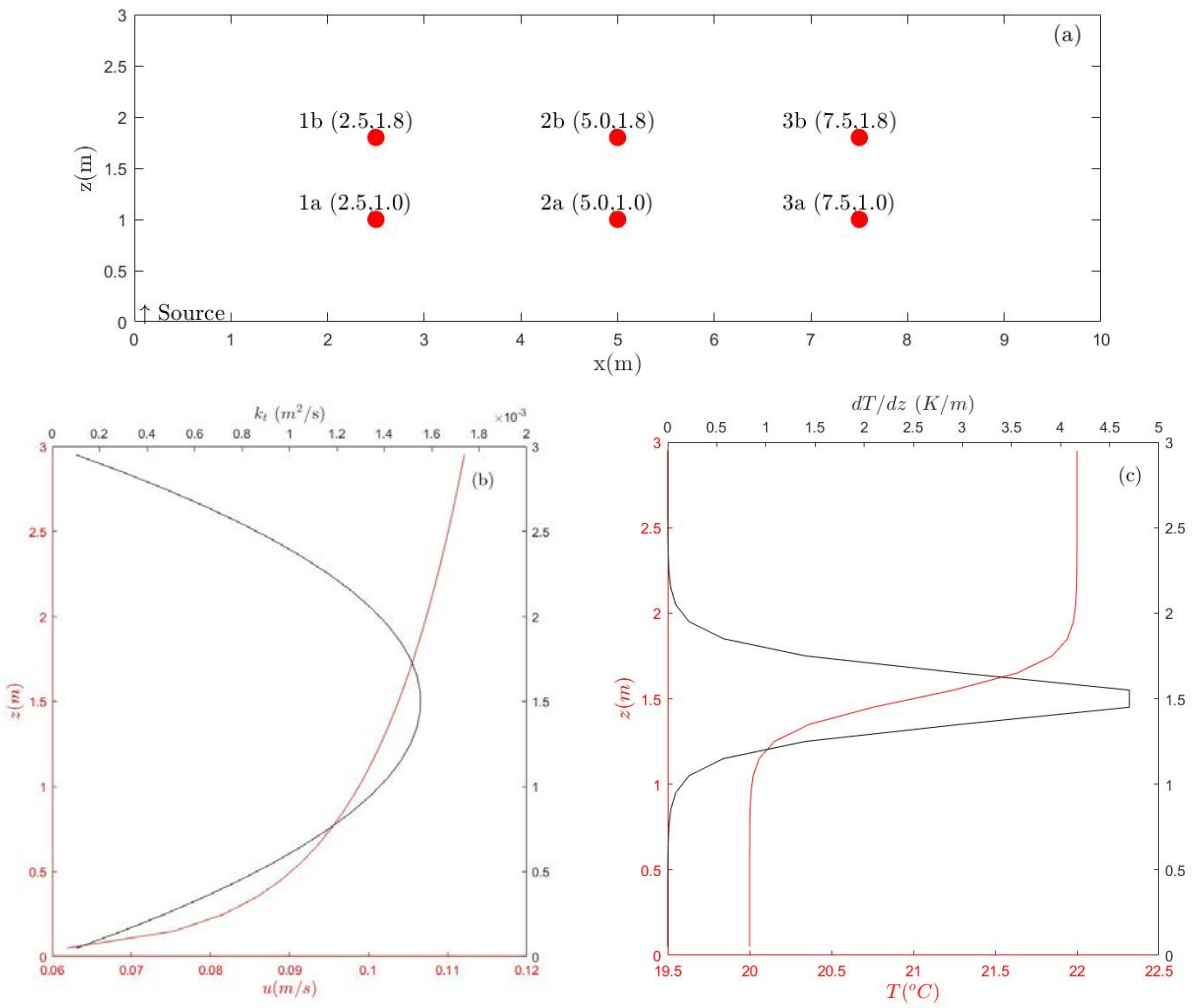

Figure 1. (a) The configuration of the modeled space; (b) The velocity profile and parabolic eddy-viscosity profile; (c) The temperature profile and the partial differentiation of temperature with respect to height.

2.1 Suspended aerosol transport model

With the assumptions including no average vertical velocity, short relaxation time, negligible horizontal diffusion, as well as turbulent fluxes following the gradient-diffusion hypothesis, the governing equation for the time averaged aerosol concentration ($\overline{C}$) in an Eulerian frame was modeled as

$$\frac{\partial \overline{C}}{\partial \mathrm{t}} + \mathrm{u}\frac{\partial \overline{C}}{\partial x} - w_p \frac{\partial \overline{C}}{\partial \mathrm{z}} = \frac{\partial}{\partial \mathrm{z}} k_t \left(\frac{\partial \overline{C}}{\partial \mathrm{z}}\right), \tag{3}$$

where u is the mean horizontal wind velocity, w_p is the settling velocity of a particle, and k_t is the eddy-diffusivity. In this model, the w_p was modeled with the stokes settling velocity. d_p was calculated with equation (2) assuming the proportional coefficient being 1. In section 3.1, d_p varied with the specified Rouse number (Ro). In section 3.2, it was assumed that R = 5 mm and h = 3 μm. k_t was modeled as ν_t/Pr_t, where ν_t is the eddy-viscosity and Pr_t is the turbulent Prandtl number (assuming to be 1).

A finite volume, first-order upwind scheme was used to model equation (3). The wind flowed from west to east, hence at time step n, it was assumed that $C_{i,j|_{eastface}} = C_{i,j}$, and $C_{i,j|_{southface}} = C_{i,j}$. At the west boundary, it was assumed that the inflow did not contain aerosols, so $C_{1,j|_{westface}} = 0$. At the top and bottom boundary, it was assumed that there were no mass fluxes, and $C_{top} = 0$. According to the mass conservation equation at the top and bottom boundary

$$Flux_{top} = -w_p C_{top} + k_t \left(\frac{\partial C}{\partial z}\right)_{top} = 0,$$

$$Flux_{bottom} = -w_p C_{bottom} + k_t \left(\frac{\partial C}{\partial z}\right)_{bottom} = -w_p C_{bottom}.$$

So, at the top and bottom cells, $k_t \frac{\partial C}{\partial z} = 0$.

2.2 Mean wind profile

The constant mean wind was modeled with a logarithmic velocity profile

$$u(z) = \frac{u_*}{\kappa} ln\left(\frac{z}{z_o}\right), \tag{4}$$

where z_o is the roughness height. By assuming the bottom boundary is smooth, z_o could be calculated as $z_o = \nu/(9u_*)$.

In this model, the height-averaged mean wind, which was defined as $U_0 = \int_{z_o}^{z} u\, dz$ was set to be 0.1 m/s, which is a common indoor wind speed without forced ventilation.

2.3 Eddy viscosity and stratification

The eddy viscosity ν_t was modeled with a parabolic zero-equation

$$\nu_t = \kappa u_* z \left(1 - \frac{z}{H}\right).$$

Temperature stratification can limit turbulence. The magnitude of the turbulence is reduced by stratification as $\nu_t|_{buoyancy} = \nu_t\left(1 + \alpha_p Ri\right)^{\gamma_p}$, where α_p = 10/3, γ_p = -3/2.

In section 3.2, to test the effect of temperature stratification, as figure (1b) shows, a temperature profile was modeled as $T = T_0 + 0.5(T_1 - T_0)(1 + tanh((z - z_s)/\delta)$, where z_s = 1.5 m and δ = 0.2m.

3. Results and discussion

3.1 Concentration profile with varied Rouse number

Particles with Ro from 25 to 90 were tested with the model. The largest corresponding d_* value when Ro = 90 is 2.6, which justifies the use of Stokes settling velocity as w_p. After nondimensionalization of equation (3), 3 dimensionless groups can be derived, which are $\tau_f u/\tilde{L}$, $\tau_f w_p/\tilde{H}$, and $\tau_f k_t/\tilde{H}^2$, where τ_f is the flow time scale, $\tilde{L}$ is the length scale, and $\tilde{H}$ is the height scale. The three corresponding time scales for horizontal advection, vertical deposition, and turbulent dispersion are $\tilde{L}/u$, $\tilde{H}/w_p$, and $\tilde{H}^2/k_t$. When the flow time scale is much larger than all the three timescales, we can reasonably argue that the system has reached equilibrium, which is more commonly referred as steady state. The horizontal advection and deposition time scales are about 2~3 mins. Even though the dispersion time scale looks large if calculated this way, since the concentration gradient change is only significant near the bottom, the length scale in this term should actually be much smaller than H.

To guarantee steady state, each case was run for 5 mins. Figure (3a) can also justify this process. The Ro for particles in section 3.2 is 33, and steady state is reached in less than 3 mins.

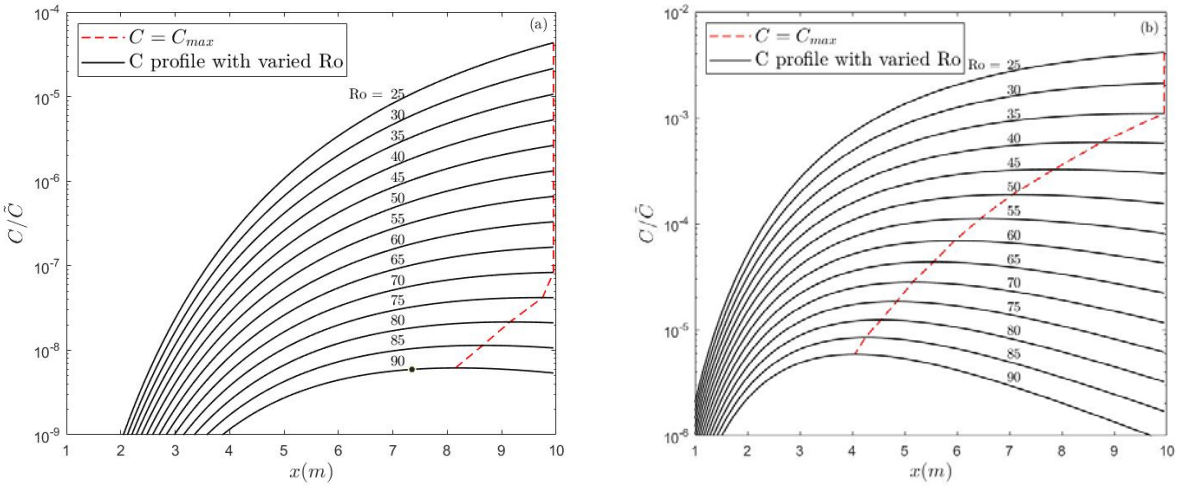

Figure 2. (a) Concentration profile at z = 1.8 m under steady state with Ro from 25 to 90; (b) Concentration profile at z = 1.0 m under steady state with Ro from 25 to 90. The read dash line is the position where the concentration is the highest with a particular Ro.

Figure (2) shows the concentration profile at z = 1.8 m and 1.0 m after 5 minutes' simulation time. The results reveal that the concentration along the x direction will reach a peak value at a position that varies with Ro. At the same height, larger aerosol droplets will reach the peak concentration in a shorter horizontal distance. And the decrease of Ro by 10 will roughly result in the decrease of peak concentration by a factor of 10. With the same Ro, aerosol droplets will reach the peak concentration in a longer horizontal distance at higher altitude, and the peak concentration at higher altitude is much lower than that at lower height.

Considering equation (3), at steady state, the unsteady term is zero, so the concentration profile is determined by the balance among the other three terms, that is, mean wind advection, inertia, and turbulent dispersion. Nondimensionalization gives us two groups: $k_t/w_p\tilde{H}$, and $u\tilde{H}/w_p\tilde{L}$, which evaluates the magnitude of turbulent dispersion versus inertia and advection versus inertia respectively. At lower height near the source, turbulent dispersion dominates the transport equation, so the particles will rise. At higher altitude, on the contrary, inertia dominates, so the particles will fall. With higher Ro, inertia will dominant the equation faster, which means the horizontal advection length scale will be shorter. This explains why the particles with larger Ro reach peak concentration at the same height earlier. At higher altitude, where velocity is also larger, the length scale needed for the particles with the same Ro to reach the balance between

turbulence dispersion and inertia will also be longer. This explains why the particles with the same Ro at higher altitude reaches peak concentration with a longer distance.

The results reveal some very important information: (1) Small particles are much more easily to be transported than larger particles, by controlling the production process of aerosol particles, it is possible to effectively limit their traveling distance. (2) The concentration distribution, to some degree, violates the common sense that 'the nearer to the source, the higher concentration would be'. Considering the finite length of indoor rooms, the real condition could be that concentration increases with horizontal distance.

3.2 Influence of Temperature stratification with continuous and pulse source

Figure (3b) shows the concentration distribution with a vertical temperature profile as figure (1c) shows after 5 minutes' simulation time. The source was continuous. As a comparison, figure (3a) shows the corresponding concentration profile without temperature stratification while keeping other factors the same as figure (3b). The result shows that a $2°C$ temperature inversion in about 0.4 meters height can significantly suppress the turbulence, hence prevent the aerosols from crossing the temperature inversion layer. But meanwhile, the concentration at lower height (<< 1 m) will become higher.

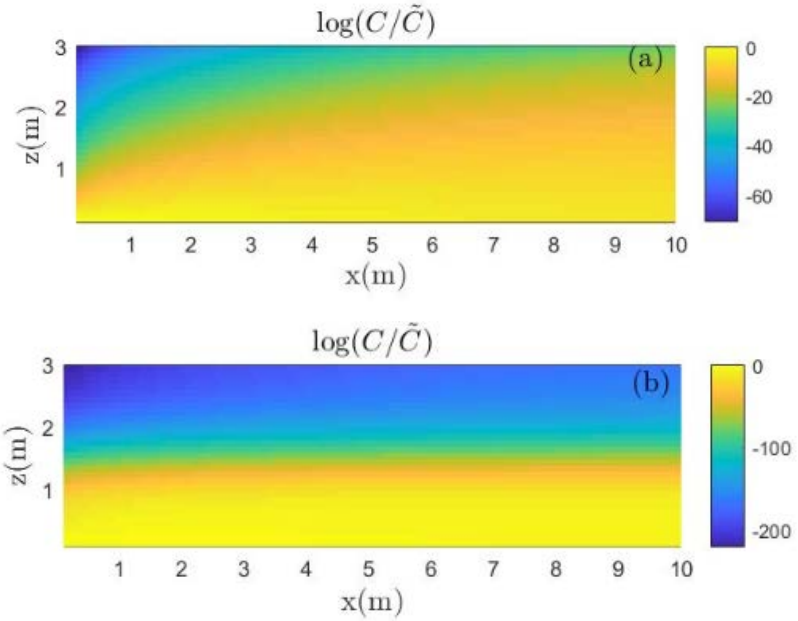

Figure 3. (a) Concentration distribution at the end of 5 min without stratification; (b) Concentration distribution at the end of 5 min with stratification.

Figure (4) shows the time series of concentration at the 6 measurement points mentioned in section 2 under 4 different source and environmental conditions.

By looking at figure (4a) and (4b), it is easy to notice that with an aerosol source at the bottom, the threat to small children is much severer than to adults. From x = 7.5 m to x = 2.5 m, the concentration of aerosols at z = 1.0 m can be higher than that at z = 1.8m by a factor of 10^2 to 10^4. The time to reach the highest concentration (for case 1a, also means reaching steady state) is approximately proportional to the horizontal distance. The vertical height does not have appreciable influence on this time scale. Pulse source case reaches the highest concentration earlier than the continuous source case. The highest concentration with pulse source is about 100 times lower than the continuous source. As section 3.1 mentioned, the highest concentration occurs at the farthest location rather on the nearest one, which deserves special attention.

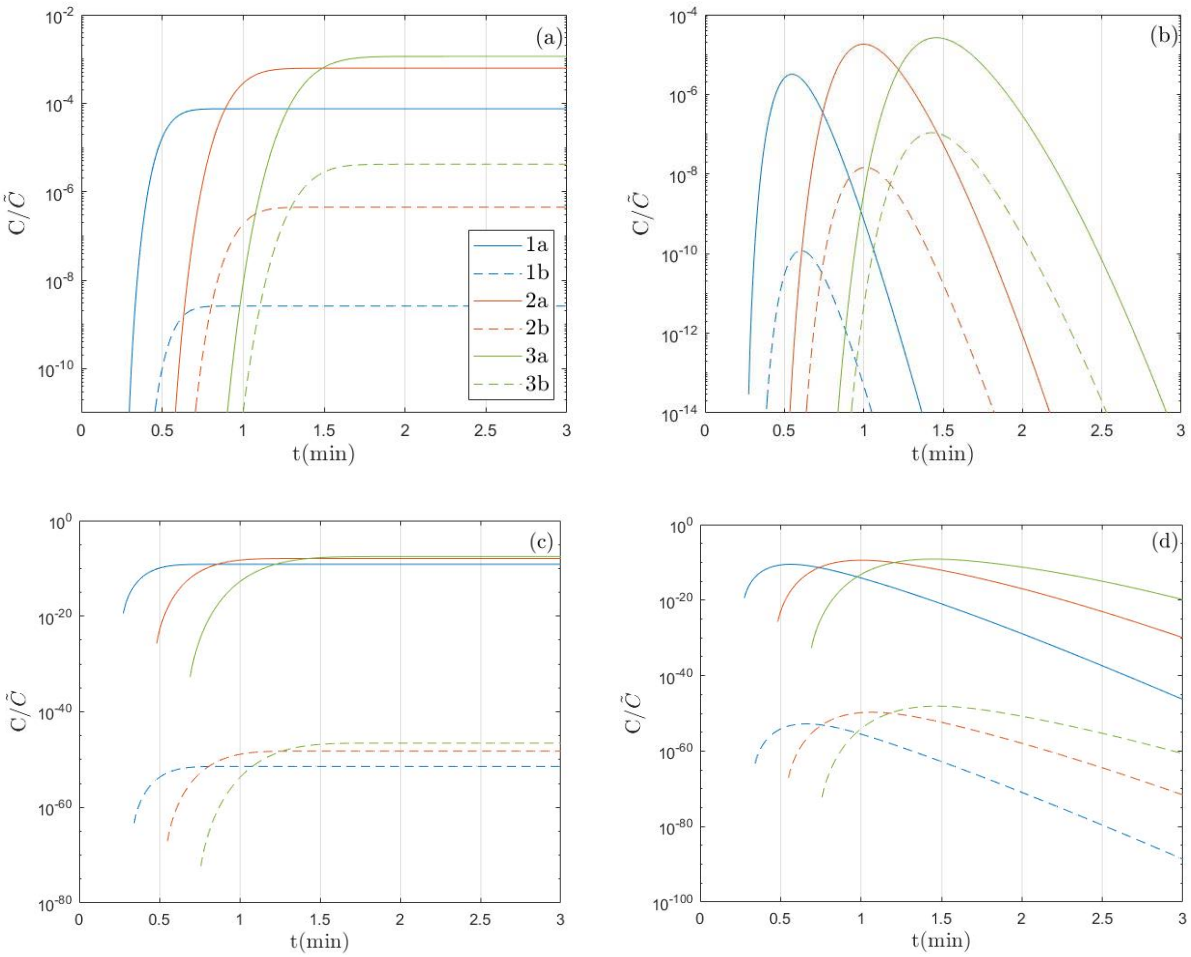

Figure 4. (a) Continuous source without stratification; (b) Pulse source without stratification; (c) Continuous source with stratification; (d) Pulse source with stratification.

By comparing figure (4a), (4b) and (4c), (4d), we can notice that the temperature inversion can decrease the aerosol concentration at z = 1.8m, which is above the inversion, to a negligible level. Meanwhile, the concentration at z = 1.0 m also decreases by some degree, although not as significant as the higher region. This result suggests the possibility of using artificial temperature inversion near the source to prevent the transport of aerosol particles.

4. Conclusions and recommendations

The results of this project can be concluded as: (1) Aerosol transport properties depend on the balance between advection, inertia, and turbulence dispersion. Near the source, turbulence dispersion dominates, resulting in the rising of aerosol particles. Far from the source, inertia dominates, resulting in the falling of aerosol particles. Advection determines the horizontal distance these particles can be transported in the flow time scale. (2) Temperature stratification can effectively constrain the generation of turbulence, hence limit the transport of aerosol partiles.

It is worthwhile to notice that this model is a 2-D time-average model, which is valuable to qualitatively test the transport properties of uniform-sized aerosol droplets under simple environmental conditions, but not precise enough to simulate the aerosol transport in a 3-D space as that in real world. To improve the simulation results, there are several improvements could be made to gain more insight. (1) The concentration gradient and velocity gradient are very large near the bottom; finer grid size could be used to increase the precision of this model. (2) A spectrum of particle sizes rather than uniform particle size could be used to achieve a more realistic simulation. (3) A 3-D model with LES method modeling the wind field could accomplish the simulation of more realistic and complex scenarios.

5. Acknowledgement

I gratefully acknowledge the support of Oliver Fringer on the development of this project. Oliver gave me invaluable suggestions and guidance on both coding and understanding physics. This project can never be finished without his generous and insightful instruction. 262G is an incredible course and I learned a lot of knowledge that is useful in all kinds of topics. I also thank the assistance of my dear classmates who are Nate, Jeremy, Cameo, Margarita, Lu and Weijia.

Reference

1. Poulain, S., E. Villermaux, and L. Bourouiba, *Ageing and burst of surface bubbles.* Journal of Fluid Mechanics, 2018. **851**: p. 636-671.
2. Lhuissier, H. and E. Villermaux, *Bursting bubble aerosols.* Journal of Fluid Mechanics, 2012. **696**: p. 5-44.
3. Poulain, S. and L. Bourouiba, *Biosurfactants Change the Thinning of Contaminated Bubbles at Bacteria-Laden Water Interfaces.* Physical Review Letters, 2018. **121**(20): p. 6.